Chirp control in the direct space-to-time pulse shaper

D. E. Leaird and A. M. Weiner

School of Electrical and Computer Engineering, Purdue University, 1285 Electrical Engineering Building, M/S 27, West Lafayette, Indiana 47907-1285

Received November 30, 1999

The dispersion properties of the direct space-to-time pulse shaper are investigated for the first time to our knowledge. We demonstrate that phase-front curvature of the input spatial profile leads to a chirp in the output temporal waveform, which one can compensate for by varying the separation between the pulse-shaping lens and slit. Furthermore, the output intensity profile remains invariant as the chirp is manipulated. These properties are fundamentally different than in the well-known Fourier-transform pulse shaper. © 2000 Optical Society of America

OCIS codes: 320.5540, 320.1590, 320.0320.

The generation of trains of femtosecond pulses, and pulse sequences, as might be used in a high-speed photonic network, was recently demonstrated with the direct space-to-time (DST) pulse shaper.[1–3] The key distinction between this geometry and the well-known Fourier-transform (FT) pulse-shaper geometry[4,5] is that the state of each pulse, either ON or OFF, in the output pulse sequence can be set by direct control of an individual spatial location. This is in contrast to the FT geometry, in which the output profile is determined by the FT of the complex spectral transmission of the spatially patterned mask. In this Letter we investigate the dispersion properties of the DST pulse shaper for the first time to our knowledge. We demonstrate that one can control chirp, and set it to zero if desired, by varying the separation of the pulse-shaping lens and the output slit while leaving the output intensity profile unaffected. Chirp control, as demonstrated here, will be important for subsequent transmission over fiber networks. Further, we find that the dispersion properties of the DST pulse shaper are fundamentally different than for the FT pulse shaper.

A schematic representation of the DST pulse shaper is shown in Fig. 1. For a complete description of the space-to-time mapping of the DST pulse shaper, refer to Ref. 3. The end result is that when the separations between the pulse-shaping lens and the grating and between the pulse-shaping lens and the output slit are both equal to the focal length of the pulse-shaping lens, f, the field just before the slit is given by

$$e_2(x,t) \propto \int \mathrm{d}\omega E_{\mathrm{in}}(\omega) S\left(\frac{2\pi x}{\beta \lambda f} - \frac{\gamma \omega}{\beta}\right) \exp(j\omega t), \quad (1)$$

where $S(k)$ is the spatial FT of the one-dimensional spatial pattern $s(x)$ that is present just after the diffraction grating; λ is the center wavelength of the input spectrum; $\gamma = \lambda/[cd\cos(\theta_d)]$ is the spatial dispersion of the diffraction grating, where c and d are the speed of light and the period of the diffraction grating (1800^{-1} mm), respectively; and the $\beta = \cos\theta_i/\cos\theta_d$ term[6] arises from the beam-size change on diffraction from the grating. $\theta_d \cong 53°$ and $\theta_i \cong 47°$ are the diffraction and the incident angles, respectively. The thin output slit samples the spatially dispersed frequency components, for example, around $x = 0$. For a sufficiently thin slit in the output field $e_{\mathrm{out}}(t)$ is given by the input pulse $e_{\mathrm{in}}(t)$ convolved with a scaled representation of the spatial profile at the grating:

$$e_{out}(t) \propto \int \mathrm{d}\omega E_{\mathrm{in}}(\omega) S\left(\frac{-\gamma \omega}{\beta}\right) \exp(j\omega t)$$

$$\propto e_{\mathrm{in}}(t) * s(-t\beta/\gamma). \quad (2)$$

The origin of chirp in this apparatus can be understood by exploration of spatial profile at the grating, $s(x)$, in more detail. Assuming that a collimated beam of radius w_{in} with a Gaussian spatial profile is incident upon the pixelation mask, $m(x)$, the imaging lenses of the mask-generation optics generate a spatial profile at the diffraction grating given by

$$s(x) = m\left(\frac{x}{\mathrm{mag}}\right) \exp\left(\frac{-x^2}{{w_g}^2}\right) \exp\left(\frac{-jk}{2R} x^2\right), \quad (3)$$

where mag is the imaging system magnification, w_g is the beam radius at the grating (also magnified by mag relative to w_{in}), and R is the phase-front radius of curvature resulting form the two imaging operations. It is this spatial profile, $s(x)$, that is mapped into the temporal domain according to expression (2). The output intensity profile exhibits a Gaussian temporal window, with the fine features determined by a scaled version of the masking function, $m(x)$. If one wishes to eliminate the Gaussian window, a diffractive optical element[7] can be used as the spot generator at the masking plane, resulting in a one-dimensional array of spots

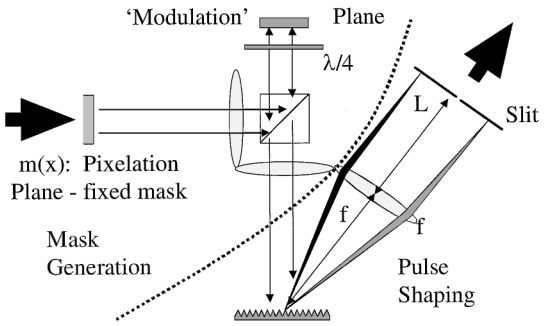

Fig. 1. Complete space-to-time shaper: Left of the dashed curve, mask-formation optics, right of dashed curve, the pulse-shaping components.

0146-9592/00/110850-03$15.00/0 © 2000 Optical Society of America

with equal intensity. Here we are most interested in the quadratic spatial phase that is present at the grating, which arises, for example, from the imaging operations shown in Fig. 1. This quadratic spatial phase is mapped into a quadratic temporal phase by the space-to-time conversion; hence a chirp (more precisely, a frequency modulation) is imparted onto the output. One way to eliminate this chirp would be to use a telescopic (not an imaging) configuration to relay the masked spatial profile onto the diffraction grating. However, even then the chirp will be eliminated only if a strictly collimated beam is present at the input to the apparatus. Any residual divergence will be mapped into a quadratic temporal phase. Because of this rigid constraint, which affects the ability to realize a truly chirp-free condition, it is important to understand other ways to control chirp in the DST apparatus.

To understand the effect of component placement on the chirp in the DST apparatus we have performed a diffraction analysis.[8] Note that Wefers and Nelson[6] and Martinez[9] have performed similar analyses for the FT shaper and the pulse stretchers, respectively—to our knowledge, ours is the first calculation for the DST geometry. The general procedure is as follows: The input spectrum, obtained as the FT of the input field $e_{\mathrm{in}}(t)$, is multiplied by the spatial profile, $s(x)$, just before the diffraction grating. The field just after the grating is given by this input field multiplied by the spatial dispersion of the diffraction grating, $\exp(-j\gamma\omega x)$. To determine a relation for the field at the apparatus output we use the field just after the grating as the input into a free-space propagation in the Fresnel regime for a distance equal to lens focal length f. The transfer function of the thin lens is then included, followed by another Fresnel propagation to the output slit a distance L away. Simplifying this expression and applying an ideal thin slit at $x = 0$ as was done for expression (2) results in an output field given by

$$e_{\mathrm{out}}(t) \propto e_{\mathrm{in}}(t) * \left\{ m\left(\frac{-t\beta}{\mathrm{mag}\ \gamma}\right) \exp\left(\frac{-t^2\beta^2}{\gamma^2 w_g{}^2}\right) \times \exp\left[\frac{-jk}{2\gamma^2}\left(\frac{\beta^2}{R} - \frac{L-f}{f^2}\right)t^2\right]\right\}. \quad (4)$$

The output intensity profile here remains identical to that of the case indicated by expression (2), in which the lens–slit separation was set at f. Expression (4) holds provided that the input pulse is short enough compared with the frequency modulation that the convolution is basically identical to the $s(x)$ contribution. However, there is now an additional quadratic temporal phase term that can be controlled by the lens–slit separation. This additional term can be set to have either a positive or a negative sign, and with proper selection of the lens–slit separation the chirp arising from the quadratic spatial phase can be canceled.

To measure the chirp of the DST apparatus, we replace the pixelation mask at the apparatus input with a single slit that can be moved transversely across the input beam. The output power spectra and intensity cross correlations measured with a reference pulse directly from the Ti:sapphire source laser (producing 100-fs pulses centered at 850 nm) are recorded as a function of input-slit position. Figure 2 shows the center wavelength of the power spectra as a function of transverse input-slit position for an imaging system magnification of 5.7. The input masking slit is 100 μm wide—we selected this width as a compromise to provide reasonably narrow power spectra and reasonably narrow intensity cross correlation. The rate of change of the center wavelength divided by the rate of change of temporal position gives a measure of the chirp. The measured chirp is 6.8 ps/nm for a configuration in which $L = f = 160$ mm. Remember from expression (4) that the chirp of the apparatus in this configuration is due to the phase-front curvature at the grating. To calculate the expected phase-front curvature at the diffraction grating we assumed a collimated beam at the pixelation plane and numerically propagated this beam through the imaging optics, utilizing *ABCD* matrices.[10] The calculation predicts a chirp of 8.5 ps/nm, in reasonable agreement with the data. The difference between the expected and the measured chirp is due to the fact that the beam at the pixelation mask is not entirely collimated.

To verify expression (4) we made a series of chirp measurements while varying the separation between the pulse-shaping lens and the output slit (L–f), with the grating–lens separation held constant at f. The output-slit width was held constant as the

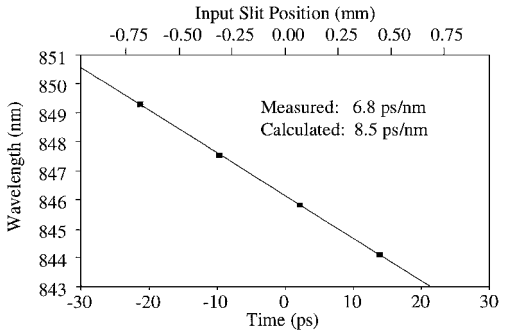

Fig. 2. Output center wavelength as a function of masking-slit position. Squares, measured center wavelength of the power spectra; solid line, linear fit.

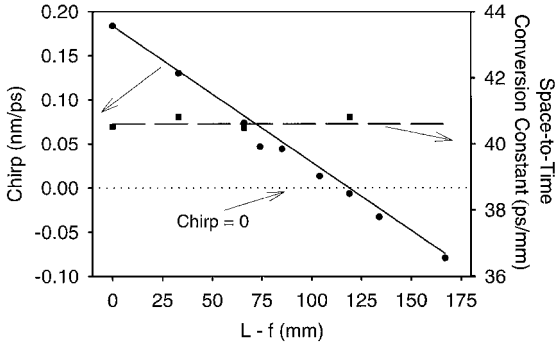

Fig. 3. Chirp and space-to-time conversion constant as a function of change in pulse-shaping lens–pulse-shaping-slit separation away from the focal length of the lens. Circles, measured chirp; squares, measured space-to-time conversion constant; solid line, calculated chirp; dashed line, calculated space-to-time conversion constant; dotted line, guide to the eye for chirp = 0.

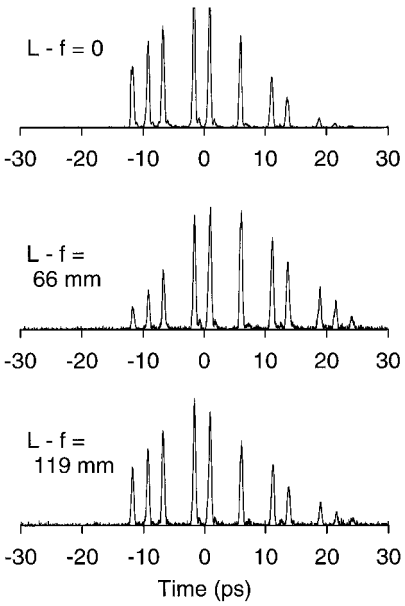

Fig. 4. Examples of optical packets generated with a fixed mask at the pixelation plane for pulse-shaping-lens–slit separations of 160, 226, and 279 mm.

grating–lens separation was changed. Figure 3 shows the results of these measurements. The chirp from the $L = f$ configuration was used as a measure of the phase-front curvature at the grating, $R = 269$ mm, and this one adjustable parameter was used to generate the calculated chirp line indicated in the figure. The calculated and the measured chirp are in excellent agreement for a large range of pulse-shaping-lens–output-slit separations. Note also that the calculation indicates that the apparatus is chirp free for a value of $L-f = 119$ mm (pulse-shaping-lens–output-slit separation of 279 mm). Figure 3 also shows the measured space-to-time conversion constant for several different pulse-shaping-lens–output-slit separations. As expected from expression (4), the space-to-time conversion constant is invariant as $L-f$ is varied. Therefore the output chirp can be controlled without affecting the output intensity profile.

To verify further that the output intensity profile is invariant with changes in $L-f$ we insert a complex pixelation mask consisting of a one-dimensional array of transparent rectangles in an otherwise opaque background at the apparatus input. Intensity cross-correlation traces of the apparatus output were recorded for several different pulse-shaping-lens–output-slit separations. Figure 4 shows the measured intensity cross correlations for lens–output-slit separations of 160, 226, and 279 mm. The $L-f = 0$ mm position corresponds to a chirp at the apparatus output that is due only to the phase-front radius of curvature at the diffraction grating. $L-f = 66$ mm corresponds to a partially compensated chirp, and $L-f = 119$ mm corresponds to a completely compensated chirp. As expected, the intensity profile is invariant with changes in L. The temporal position of each pulse in the output train is determined by the space-to-time mapping from the pixelation mask, and the roll-off in the train is due to the finite beam size at the pixelation mask.

Finally, a brief comment about the system power throughput is in order. A previous publication[3] commented on the ideal optical power throughput in the case $L = f$. Here we have performed simple measurements for the case of an open window pixelation pattern that indicate that the transmitted power remains approximately constant as the longitudinal position of the output slit (L) is varied. This result is consistent with a simple scaling argument: As the output slit is scanned for chirp compensation, the peak spectral intensity varies inversely with the chirp but the spectral width varies with the chirp, so the output power is constant.

In summary, we have shown that chirp on the output of the DST pulse shaper can be accurately predicted and controlled. Proper selection of the lens–pulse-shaping-slit separation permits the apparatus to be chirp free. This is in contrast to the well-known FT pulse-shaping geometry, in which the apparatus chirp is adjusted by means of changing the grating–lens separation. Further, the output intensity profile is invariant as the chirp of the DST pulse shaper is varied.

This material is based on work supported by, or in part by, the U.S. Army Research Office under contract DAAG55-98-1-0514. D. E. Leaird's e-mail address is leaird@purdue.edu.

References

1. C. Froehly, B. Colombeau, and M. Vampouille, in *Progress in Optics*, E. Wolf, ed. (North-Holland, Amsterdam, 1983), pp. 65–153.
2. Ph. Emplit, J.-P. Hamaide, and F. Reynaud, Opt. Lett. **17,** 1358 (1992).
3. D. E. Leaird and A. M. Weiner, Opt. Lett. **24,** 853 (1999).
4. A. M. Weiner, J. P. Heritage, and E. M. Kirschner, J. Opt. Soc. Am. B **5,** 1563 (1988).
5. A. M. Weiner, Prog. Quantum Electron. **19,** 161 (1995).
6. M. M. Wefers and K. A. Nelson, IEEE J. Quantum Electron. **32,** 161 (1996).
7. R. L. Morrison, S. L. Walker, and T. J. Cloonan, Appl. Opt. **32,** 2512 (1993).
8. J. W. Goodman, *Introduction to Fourier Optics* (McGraw-Hill, New York, 1968).
9. O. E. Martinez, J. Opt. Soc. Am. B **3,** 929 (1986).
10. J. T. Verdeyen, *Laser Electronics* (Prentice-Hall, Englewood Cliffs, N.J., 1995).